ELSEVIER

Journal of Fluids and Structures 23 (2007) 1231–1250

JOURNAL OF FLUIDS AND STRUCTURES

www.elsevier.com/locate/jfs

The genetically optimized tunnel-entrance hood

M.S. Howe*

College of Engineering, Boston University, 110 Cummington Street, Boston, MA 02215, USA

Received 6 October 2006; accepted 17 June 2007

Abstract

A numerical procedure is investigated for optimizing the design of tunnel-entrance hoods used for controlling the compression wave generated when a high-speed train enters a tunnel. Long hoods are required for long tunnels and train speeds exceeding about 350 km/h. The hood must minimize the maximum pressure gradient across the compression wave-front by taking advantage of the pressure-release provided by open windows distributed along one or both of its walls. The compression wave produced by the train can be evaluated by means of a rapid computational scheme devised and validated against experiment. Optimization is achieved by representing a possible distribution of windows by a binary string. The individuals in an initial, random population of such strings are allowed to 'mate' and evolve by 'natural selection' through several generations towards an optimal configuration by application of a genetic algorithm. The genetically fittest hood is associated with the minimum possible maximum pressure gradient for prescribed values of the train speed and hood dimensions. The algorithm yields an optimal design from among a theoretically unlimited number of possibilities; it can also supply near-optimal, smoothly varying window distributions (or optimize the variation in width of a long slit-like window in the hood wall) satisfying additional constraints imposed by the designer.

Keywords: Genetic algorithm; High-speed train; Shinkansen; Tunnel-entrance hood; Compression wave; Micro-pressure wave

1. Introduction

The subjective characteristics of the compression wave generated when a high-speed train enters a tunnel are governed principally by the shape of the wavefront profile (Gawthorpe, 1978; Gregoire et al., 1997; Iida et al., 1996; Ito, 2000; Maeda et al., 1993; Matsuo et al., 1997; Noguchi et al., 1996; Ozawa et al., 1976,1991; Ozawa and Maeda, 1988a; Woods and Pope, 1976). The overall pressure rise across the wave-front varies roughly as the square of the train speed U, and can exceed 2% or 3% of atmospheric pressure, but the wave profile depends on the shapes of both the train nose and tunnel portal (Gregoire et al., 1997; Iida et al., 1996; Ito, 2000; Maeda et al., 1993; Matsuo et al., 1997; Noguchi et al., 1996; Ozawa and Maeda, 1988a; Ozawa et al., 1978, 1991; Peters, 2000). An acoustic pulse (the *micro-pressure* wave) is radiated from the far end of the tunnel when the compression wave arrives. The pulse strength is proportional to the slope of the compression wave-front and varies as U^3 for short tunnels; it can be large enough

*Tel.: +1 617 484 0656; fax: +1 617 353 5866.
E-mail address: mshowe@bu.edu

0889-9746/$ - see front matter © 2007 Elsevier Ltd. All rights reserved.
doi:10.1016/j.jfluidstructs.2007.06.005

to cause annoying 'rattles' in building structures close to the tunnel exit. The problem is often exacerbated by the use of acoustically smooth, concrete slab tracks in long tunnels, because reduced damping promotes nonlinear steepening of the front.

The influence of wave-front steepening can be greatly reduced by installing a tunnel entrance 'hood' (Ozawa and Maeda, 1988a,b; Ozawa et al., 1978, 1991). This is a thin-walled extension of the tunnel, usually of larger cross-sectional area, and with open 'windows' distributed along its length. High pressure air is forced through the windows by the train, producing modifications in both the initial 'rise time' and profile of the compression wave. Very large increases in the effective thickness of the wave-front can be achieved by proper choice of the spacing and sizing of the windows. An optimal wave-front profile should be long enough to vitiate the effects of wave steepening in a long tunnel; the ideal profile exhibits linear growth over a wavefront thickness ~(hood length)$/M$ determined by the time of passage of the train nose through the hood, where $M = U/c_0$ is the train Mach number (c_0 being the mean sound speed in air).

Hood design is usually based on model scale testing using experimental apparatus of the kind illustrated schematically in Fig. 1 (typically $\sim\frac{1}{127}$ full scale), and on numerical modelling (Ozawa and Maeda, 1988a,b; Ozawa et al., 1978, 1991; Maeda et al., 1993; Howe, 2005; Howe and Iida, 2003; Howe et al., 2000, 2003a,b, 2006). A common configuration involves a circular cylindrical tunnel fitted with a cylindrical, coaxial hood, into which an axisymmetric model train is projected along a tightly stretched wire guide at speeds up to 500 km/h. The initial form of the compression wave is measured using flush-mounted pressure sensors in the tunnel walls at a distance of 1–2 m from the junction with the hood. The Reynolds number is sufficiently large that dynamic similarity with full scale is achieved during the initial stages of wave formation for a given value of M. However, flow separation to the rear of the train nose causes a progressive, Reynolds number dependent, pressure increase to the rear of the wave front; this can be attributed to a distributed dipole source whose strength per unit length of train is equal to the frictional drag on the train and tunnel.

A very efficient numerical scheme is described by Howe et al. (2006) for predicting the initial compression wave (prior to the onset of nonlinear steepening) for axisymmetric model scale experiments in terms of a prescribed tunnel-hood geometry and window distribution. The procedure includes the influences on wave formation of (i) the hood-tunnel junction and the consequent temporary 'trapping' of wave energy in the hood by multiple reflections, (ii) the formation of air jets exhausting from the hood windows, and (iii) the frictional drag on the train and tunnel walls. It has been validated by comparison with a series of experiments conducted over a period of years (Howe, 2005; Howe and Iida, 2003; Howe et al., 2000, 2003a,b, 2006; Winslow et al., 2005) at speeds U up to 425 km/h.

There is an obvious practical need, however, for an 'inverse' algorithm that determines the optimal hood dimensions and distribution and sizing of the hood windows in terms of prescribed values of the train speed U and the train nose characteristics. The need is particularly urgent at the higher operating speeds of proposed newer trains (U~500 km/h for *Maglev* designs), which are expected to spend at least 50% of a typical journey within a succession of long tunnels. It is conjectured that hoods as long as 200 m with many windows will then be necessary to counter nonlinear wave-front steepening. In these circumstances it should be possible to greatly reduce the number of lengthy hood validation tests by selecting candidate designs on the basis of preliminary numerical studies.

The numerical method of Howe et al. (2006) can be run in a few seconds on a modern desk-top computer. It is readily incorporated into an inverse algorithm that seeks and evaluates candidate hood designs. The procedure can be automated in the form of a genetic algorithm (Goldberg, 1988; Michalawicz, 1992; Coley, 1999; Vose, 1999) that determines the optimum by 'natural selection' (Fisher, 1958), and in this paper the feasibility of this approach is assessed by application to model scale axisymmetric configurations at $U = 360$ km/h, which will be typical of higher speed trains in the near future. The actual procedure to be used is a 'simple genetic algorithm' (Coley, 1999) extended in the manner described by Carroll (1996).

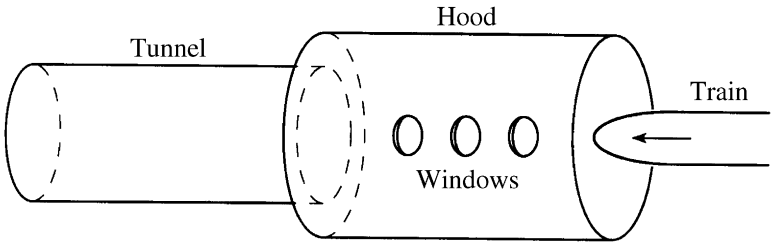

Fig. 1. Schematic experimental configuration involving a model scale train entering an axisymmetric cylindrical tunnel and entrance hood with windows.

Formulae relating to the prediction method of Howe et al. (2006) are briefly discussed in Section 2 and collected together for reference in Appendix A. The genetic algorithm is described in Section 3. Application is made to two different axisymmetric tunnel-hood configurations in Sections 4 and 5.

2. Calculation of the compression wave

2.1. Pressure source mechanisms

The compression-wave prediction scheme of Howe et al. (2006) is applicable to configurations of the type illustrated in its simplest form in Fig. 2, in terms of which the following brief resumé of the principal mechanisms contributing to wave formation can be given.

The train nose can be regarded as a combination of a monopole source, of strength equal to the rate at which air is displaced by the advancing train, and a 'drag' dipole equal in magnitude to the net pressure force on the nose produced by the pressure rise in front of the train. Both sources are localized to the nose region where the cross-sectional area $\mathscr{A}_T$, say, of the train is varying.

The initial pressure rise p_E in front of the train occurs as the monopole and dipole sources first interact with the hood portal, as the nose crosses the hood entrance plane E (Fig. 2). This disturbance propagates as a plane wave ahead of the train and subsequently interacts with windows W and with the junction J of the hood and tunnel before the arrival of the train (Howe et al., 2000, 2003a,b). At J the wave is partially transmitted into the tunnel and partially reflected back into the hood. The subsequent interaction of reflected waves with the train can be ignored provided the 'blockage' $\mathscr{A}_0/\mathscr{A}_h$ is less than about 0.2, where $\mathscr{A}_0$ is the uniform cross-sectional area of the train to the rear of the nose, and $\mathscr{A}_h$ is the cross-section of the hood; this is the usual situation at full scale. However, almost perfect total reflection occurs at the hood portal E, with reflection coefficient ~ -1, and the wave is then multiply reflected from the ends of the hood. Each reflection from the junction J is accompanied by the transmission of a fraction of the wave energy into the tunnel, such that, after four or five back-and-forth reflections of p_E within the hood, most of the initial wave energy has been transmitted into the tunnel.

A second pressure wave p_J, say, is generated when the train nose reaches the junction J. This propagates into the tunnel as a compression wave and towards E as an expansion wave. The latter component is multiply reflected within the hood before being wholly transmitted into the tunnel, where it contributes to the tail end of the compression wave-front.

These interactions become more complicated in the presence of windows. In the case of a single window (W in Fig. 2), the arrival of p_E forces air out of the window, forming a high speed jet whose velocity can increase to as much 50% of the train speed U. The window behaves as a negative acoustic source (controlled by the inertia of the jet) producing an expansion wave p_W that initially propagates from the window with equal amplitudes in both directions in the hood. In particular, it causes an effective reduction in the amplitude of the compression wave p_E transmitted past the window. The subsequent incidence on the window of waves multiply-reflected from the ends of the hood produce variations in

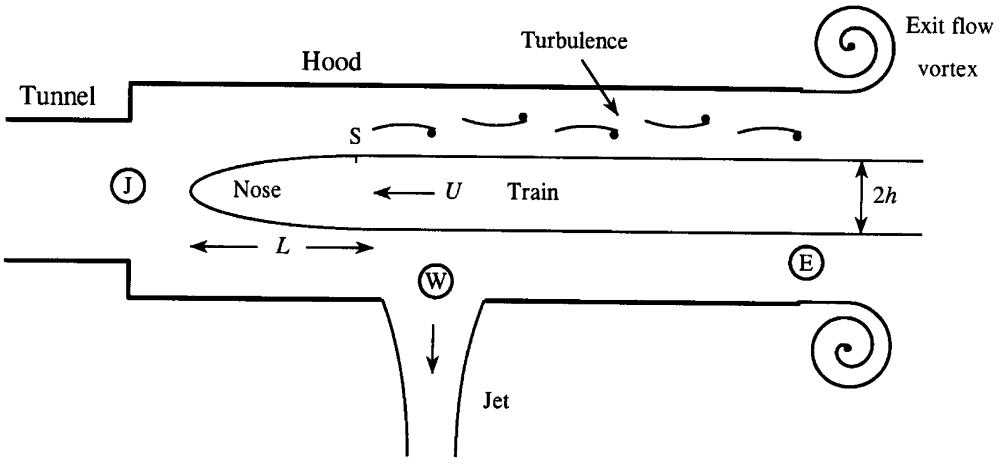

Fig. 2. The principal flow sources and interactions contributing to compression wave generation.

the window source strength, which tends to remain significant until the train nose passes the window (Howe, 2005; Howe et al., 2003b). Similar remarks are applicable to a hood with several windows: each window behaves as a monopole source of waves, and the volume velocities ('source strengths') of the different windows are coupled by the pressure waves reflecting back-and-forth within the hood.

In addition to these waves turbulence between the tunnel walls and the train (to the rear of the point S in Fig. 2) generates a pressure component p_D that accounts for a gradual pressure rise to the rear of the main compression wave front (Howe and Iida, 2003). The turbulence forms a dipole, surface source whose overall strength is equal to the drag on the train and wall, and it therefore increases approximately linearly with time, being proportional to the length of train within the tunnel and hood. A much smaller pressure pulse attributable to the large vortex formed just outside the hood portal (Fig. 2) (Auvity and Bellenoue, 1998; Auvity et al., 2001; Fukuda et al., 2003) can usually be ignored (Howe and Iida, 2003).

2.2. The model scale configuration

The superposed pressures p_E, p_J, p_W, p_D, appropriately modified by reflections from the ends of the hood, dominate the shape of the compression wave front. They will be calculated for the axisymmetric arrangement shown in Fig. 3, involving a model scale tunnel in the form of a circular cylindrical duct of internal radius R fitted axisymmetrically with a thin-walled, circular cylindrical hood of internal radius R_h, length ℓ_h and wall thickness ℓ_w, with an *unflanged* opening. The origin of coordinates (x, y, z) is taken at the centre O of the hood entrance plane, with the negative x-axis coinciding with the common axis of symmetry of the tunnel and hood.

There are N windows distributed in a single row along one side of the hood, such that the kth window has area A_k and its centroid is at $(x_k, 0, R)$, $-\ell_h < x_k < 0$; the figure illustrates this for $N = 3$. In general $A_k \ll \mathscr{A}_h = \pi R_h^2 \equiv$ cross-sectional area of the hood. In a first approximation predictions are independent of the window *shape*: the influence of a rectangular window of axial and azimuthal lengths, respectively, equal to ℓ_x and ℓ_θ is well represented by that of a circular window of equal area provided ℓ_x and ℓ_θ are of comparable magnitudes (Howe et al., 2003b; Howe, 2005). Long, slit-like windows can be approximated by a linear array of small circular windows.

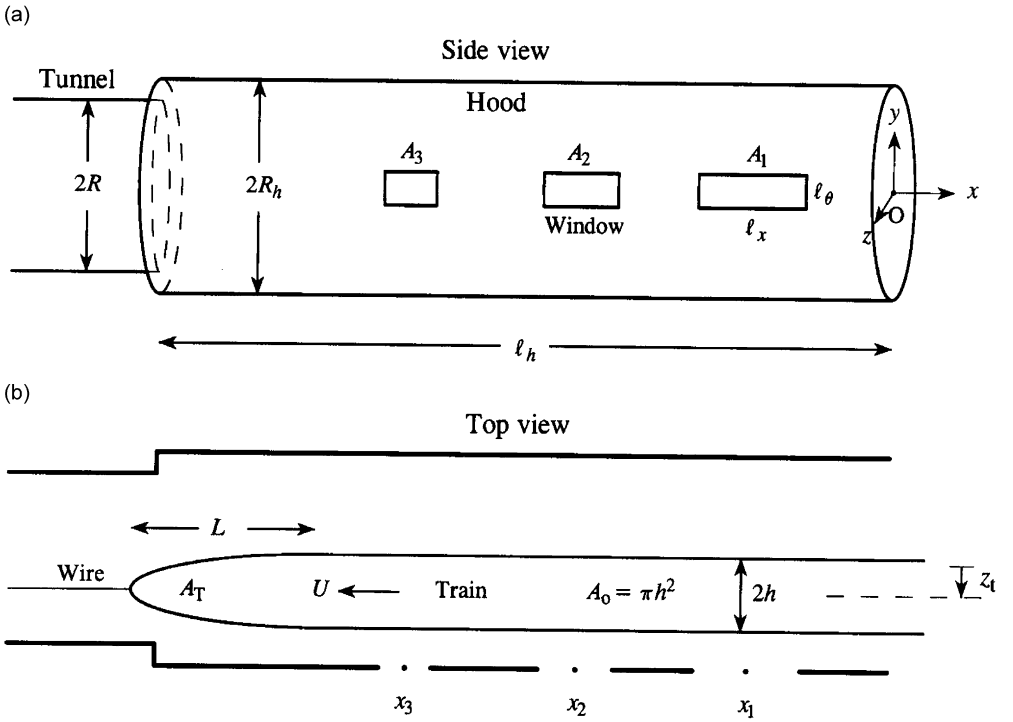

Fig. 3. Coefficients defining the hood, tunnel and axisymmetric train: (a) 'side' view from the direction of the positive z-axis; (b) 'top' view from the direction of the positive y-axis.

The model train is projected into the hood along a stretched wire passing smoothly through a cylindrical channel bored along the train axis. The train speed is uniform and equal to U, and the time origin is adjusted to ensure that the nose first cuts the hood entrance plane $x=0$ at time $t=0$. The 'top' view in Fig. 3(b) shows the wire displaced a distance $z_t>0$ from the tunnel axis *towards the windows* (in the z-direction). The two cases $z_t \gtrless 0$ therefore correspond, respectively, to a train travelling along a track that is 'near' or 'far' from the windows.

The circular cross-section of the train has constant radius h and area $\mathscr{A}_0=\pi h^2$ except within a distance L of the front of the train, where the area $\mathscr{A}_T(s)$ varies with distance s from the nose tip. In this paper the nose is assumed to be ellipsoidal with radius

$$r=h\sqrt{\frac{s}{L}\left(2-\frac{s}{L}\right)},\quad 0<s<L. \tag{2.1}$$

Then, near the front of the train

$$\frac{\mathscr{A}_T(s)}{\mathscr{A}_0}=\begin{cases}\dfrac{s}{L}\left(2-\dfrac{s}{L}\right), & 0<s<L,\\ 1, & s>L.\end{cases} \tag{2.2}$$

For numerical purposes this formula can be assumed to apply over $0<s<+\infty$, because the expansion wave produced when the 'tail' of the train enters the hood is of no concern in the present discussion. We shall also take the following values for the nose 'aspect ratio' and the tunnel blockage:

$$\frac{L}{h}=3,\quad \frac{\mathscr{A}_0}{\mathscr{A}}=0.2, \tag{2.3}$$

where $\mathscr{A}=\pi R^2$ is the cross-sectional area of the tunnel.

2.3. Compression wave formulae

The disturbance in front of the train, in the uniform tunnel in $x<-\ell_h$, rapidly assumes the form of a plane acoustic wave of pressure $p(t+x/c_0)$ propagating towards $x=-\infty$, where

$$p\left(t+\frac{x}{c_0}\right)=p_E(x,t)+p_J(x,t)+p_D(x,t)+p_W(x,t)\quad (x<-\ell_h). \tag{2.4}$$

Detailed formulae for each term on the right-hand side are given and discussed in Howe et al. (2006). Those required by the genetic algorithm to be described in Section 3 are summarized in Appendix A, and may be consulted when necessary.

3. The optimization problem

3.1. Pressure gradient attenuation by an unvented hood

The effectiveness of a hood is assumed to be determined by the reduction achieved in the maximum value $(\partial p/\partial t)_{\max}$ of the compression wave 'pressure gradient' $\partial p/\partial t$ relative to that in the absence of the hood. Consider first a circular cylindrical tunnel of radius R with no hood (Fig. 3(a) with $R_h=R$ and no windows). Let the train be defined as in Section 2.2; only the components p_E and p_D of (2.4) are nonzero. Fig. 4(a) shows typical profiles of the compression wave pressure p and pressure gradient $\partial p/\partial t$ predicted by the formulae given in Appendix A at position x (<0) ahead of the train within the tunnel, plotted as functions of the nondimensional retarded time $U[t]/R\equiv U(t+x/c_0)/R$. These predictions take no account of nonlinear steepening and therefore represent the initial waveform, shortly after generation by the entering train.

The calculations have been performed for the train defined in Section 2.2 when $U=360\,\mathrm{km/h}$ and when the track offset $z_t=0.4R$. Here and henceforth the following mean physical parameter values are assumed:

$$\left.\begin{aligned}&c_0=340\,\mathrm{m/s}\\ &\rho_0=1.23\,\mathrm{kg/m^3}\quad\text{(mean density of air)}\\ &\mu=0.053\quad\text{(friction factor)}\end{aligned}\right\}. \tag{3.1}$$

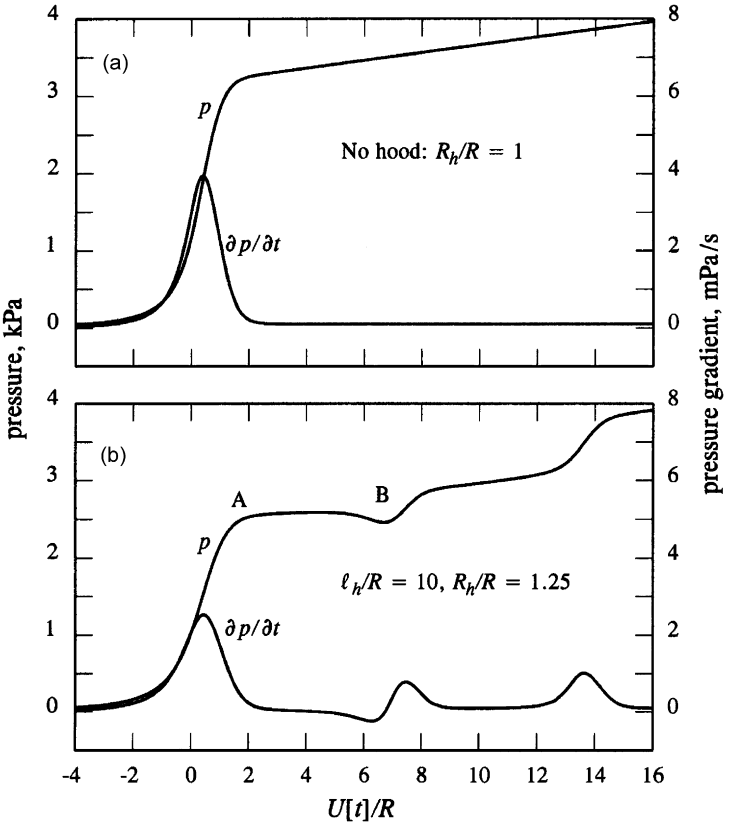

Fig. 4. Calculated time dependances of the compression wave pressure p and pressure gradient $\partial p/\partial t$ for the model train defined by (2.1)–(2.3) subject to conditions (3.1) when: (a) there is no hood; (b) the hood length $\ell_h = 10R$ and $R_h/R = 1.25$.

The train nose pierces the entrance plane $x = 0$ of the tunnel at $t = 0$. The initial rapid pressure rise of about 3.2 kPa across the wave-front (determined by the component p_E of (2.4)) occurs over a time $\sim 2R/U$; the slow, linear increase in pressure behind the wave-front is produced by the frictional pressure component p_D. The maximum value of the pressure gradient $\sim$3.95 MPa/s is attained at $U[t]/R = 0.39$.

The corresponding plots in Fig. 4(b) show how these predictions are altered when the tunnel is fitted with an *unvented* hood of length $\ell_h = 10R$ and radius $R_h = 1.25R$. The same overall pressure rise is now achieved in distinct stages. The initial rise at the wave-front (A in the figure) is reduced to about 2.5 kPa (a fraction $\sim \mathscr{T}_J \mathscr{A}/\mathscr{A}_h = 2\mathscr{A}/(\mathscr{A}_h + \mathscr{A}) = 0.78$ of its value in the absence of the hood; see Appendix A). Wave energy is temporarily trapped in the hood by reflections from its ends; the step-like pressure rises seen in the figure can be attributed to the effects of these reflections and also to secondary waves generated by the train nose as it passes the junction (Howe et al., 2003a). The complicated behaviour at B, for example, arises as follows: the initial small pressure dip is caused by a *negative* contribution attributable to the initial pressure rise at A after reflection at the junction and again at the hood entrance after a total time delay $\sim 2(\ell_h + \ell_E)/c_0$ (therefore received at x at $U[t]/R \sim 2M(\ell_h + \ell_E)/R = 6.2$) where $\ell_E = 0.763R$ is the 'end correction' of the hood (see Eq. (A.1) of Appendix A); the subsequent pressure *rise* at B is produced by a pressure pulse generated by the train nose as it passes the junction at time $\sim \ell_h/U$ after entering the hood. This is received at $x\ (< -\ell_h)$ within the tunnel after a delay $\sim -(\ell_h + x)/c_0$, i.e. at $U[t]/R \sim (1 - M)\ell_h/R = 7.06$. However, the maximum pressure gradient still occurs at the wave-front, but is reduced to 2.53 MPa/s at $U[t]/R = 0.45$.

It should now be evident that, for a given value of the train Mach number M, increasing the length of the hood beyond a certain critical value can never lead to further reductions in $(\partial p/\partial t)_{max}$. In the present case $M = 0.29$ and $(\partial p/\partial t)_{max}$ always exceeds about 2.53 MPa/s. Indeed, the wave-front is generated at the hood entrance *exactly* as if the train is entering a uniform tunnel of infinite length, and the first step increase always has the structure described in the previous paragraph (a dip followed by a rise produced by the passage of the nose past the junction)

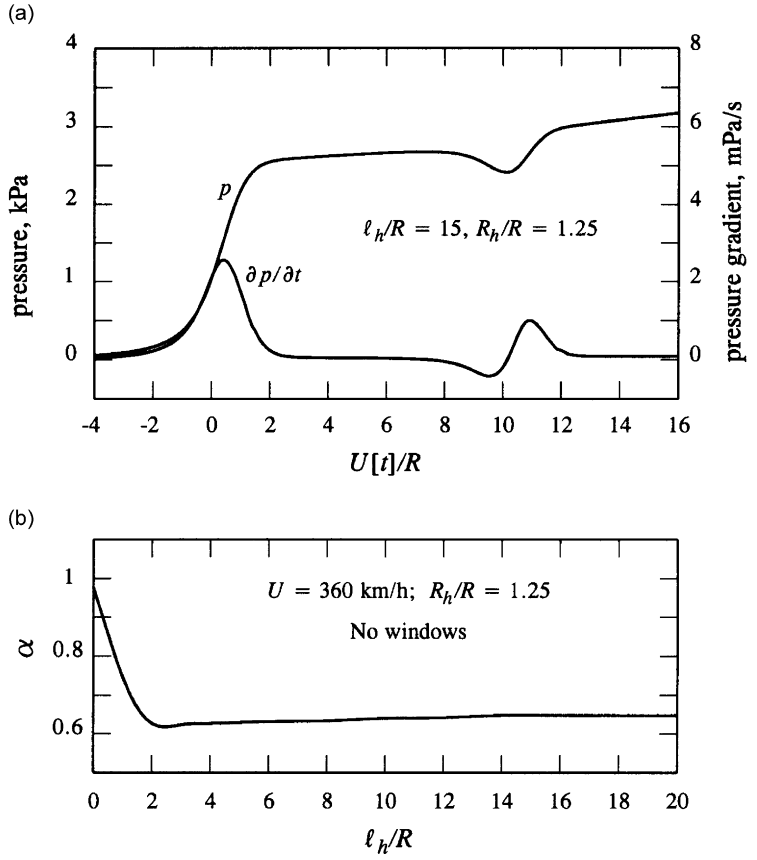

Fig. 5. (a) Calculated time dependances of the compression wave pressure p and pressure gradient $\partial p/\partial t$ for the model train defined by (2.1)–(2.3) subject to conditions (3.1) for a hood of length $\ell_h = 15R$ and for $R_h/R = 1.25$. (b) Variation of the attenuation α of (3.2) with hood length when $U = 360\,\text{km/h}$ and $R_h/R = 1.25$.

because, when $\ell_E \ll \ell_h$,

$$\frac{2M(\ell_h + \ell_E)}{(1-M)\ell_h} \sim \frac{2M}{(1-M)} = \text{a constant independent of } \ell_h.$$

Fig. 5(a) illustrates this conclusion when the hood length is increased to $\ell_h = 15R$.

The attenuation α produced by a hood is defined by

$$\alpha = \frac{\text{maximum pressure gradient}}{\text{maximum pressure gradient when the hood is absent}}. \tag{3.2}$$

Fig. 5(b) shows the calculated dependence of α on hood length ℓ_h/R for $U = 360\,\text{km/h}$ ($M = 0.29$) and $R_h/R = 1.25$. For a hood of zero length ($\ell_h = 0$) the portal consists of a circular cylindrical exit of radius R fitted with a 'flange' of radius $1.25R$, in which case $\alpha \approx 0.98$. As ℓ_h increases from zero the maximal attenuation is attained rapidly for a relatively short hood with $\ell_h/R \approx 2$. There is little or no practical benefit in using an unvented hood of greater length. Further increases in the attenuation can be achieved by increasing the hood radius or by the introduction of windows. The optimization procedure to be discussed aims to obtain maximal hood attenuation by proper choice of the distribution and sizing of windows.

3.2. The genetic algorithm

In the model scale experiment the basic hood geometry is defined by prescribed values of ℓ_h/R and $\mathscr{A}_h/\mathscr{A}$; in addition, there are N windows with centroids at axial locations x_k evenly spaced along the wall of the hood. The train

speed U, blockage $\mathscr{A}_0/\mathscr{A}$, nose aspect ratio L/h and track offset z_t are also prescribed. The genetic algorithm will be used to determine the distribution of window cross-sectional areas A_k that minimizes the maximum value of the compression wave pressure gradient $\partial p/\partial t$ radiated into the tunnel. This distribution will define the 'optimal hood'.

The algorithm starts by selecting a random population (the first 'generation') of $N_{\rm pop}$ possible hood–window distributions. Each distribution is represented by a binary string obtained by concatenating N substrings of equal length $N_{\rm sub}$; the kth substring is a binary number that decodes to the fractional area $A_k/\mathscr{A}$ of the kth window. The precision with which window areas are determined is increased by increasing the substring length $N_{\rm sub}$. The 'fitness' of a distribution is defined by the minimum value of the predicted maximum pressure gradient $(\partial p/\partial t)_{\max}$, i.e.

$$\text{fitness} = \text{maximum value of } \left[-\left(\frac{\partial p}{\partial t}\right)_{\max}\right]. \tag{3.3}$$

The fitness of each member of the population is calculated using the prediction formulae in Appendix A. The optimal window distribution is determined iteratively by allowing successive generations of hood-window populations to evolve by a process of 'natural selection' that aims to maximize population fitness (Fisher, 1958). Procedures for doing this differ in many small details (Goldberg, 1988; Michalawicz, 1992; Carroll, 1996; Coley, 1999; Vose, 1999); in this paper $N_{\rm pop}$ is required to be *even*, and each new generation is determined from the previous one by application of the following rules:

(i) *Reproduction*: $\frac{1}{2}N_{\rm pop}$ pairs of members of the current generation are selected as 'parents' for mating. The selection probability of each member is the ratio

$$\frac{\text{member fitness}}{\text{total population fitness}}.$$

(ii) *Mating*: 'Single point cross-over' is applied with probability $P_{\rm cross} = 0.6$ to each pair selected for mating to produce two offspring. To do this a 'cut' is made at random at the same place in the two binary strings of the parents; the offspring are then obtained by interchanging between the strings the binary digits on, say, the left side of each cut. In cases where cross-over is not applied (which occurs with probability $1 - P_{\rm cross}$) the two parents go forward (as 'offspring') without change.

(iii) *Mutation*: Each bit in the binary string representation of all offspring is reversed ($1 \to 0$ or $0 \to 1$) with probability $P_{\rm mut} = 1/(\text{binary string length})$.

(iv) *Creep is applied to each of the N substrings of an offspring*: 1 is added or subtracted at random from the least significant bit of the substring with probability

$$P_{\rm creep} = \frac{\text{binary string length}}{N \times N_{\rm pop}} = \frac{N_{\rm sub}}{N_{\rm pop}}.$$

(v) *Elitism*: If the fitness of the fittest (the 'elite') member of the previous generation exceeds the fitness of each offspring then one offspring chosen at random is replaced by the elite member.

(vi) *New generation*: The surviving population of offspring define the new generation.

Rules (i)–(vi) are applied repeatedly until a suitable termination condition is satisfied. In practice this means until the elite member ceases to change. For hoods with many windows (20 or more) there is a multitude of different window distributions that correspond to local minima in the maximum pressure gradient; it is then necessary to run the algorithm several times with different population sizes and substring lengths. In this way an excellent estimate can be obtained of the optimum window distribution, or at least of the minimum achievable pressure gradient.

4. Hood optimization when $R_h/R = 1$

4.1. Unconstrained windows

The simplest optimization problem occurs for the limiting case $R_h = R$. The numerical scheme of Appendix A yields the most accurate predictions when the fractional window areas $A_k/\mathscr{A}$ are small, less than about 0.2, say. We shall examine predictions of the genetic algorithm when $0 < \ell_h/R < 20$.

It soon becomes evident (for each fixed value of ℓ_h/R) that there generally exist many different window distributions with a minimum value of $(\partial p/\partial t)_{\max}$ close to the global minimum. This accords with the experimental observation that many different window arrangements can lead to similar modifications of the initial compression wave profile (Iida, 2005).

The calculations are performed by taking the windows to be evenly spaced along one of the hood walls (of thickness $\ell_w = 0.06R$), according to the formula

$$-x_k = \frac{\ell_h}{N}\left(k - \frac{1}{2}\right), \quad 1 \leqslant k \leqslant N. \tag{4.1}$$

Figs. 6 and 7 illustrate typical optimal waveforms for 'far' windows for the two cases summarized in Table 1.

The attenuation α in the final column is calculated from the formula

$$\alpha = \frac{(\partial p/\partial t)_{\max}}{3.95}, \tag{4.2}$$

where $(\partial p/\partial t)_{\max}$ is the maximum pressure gradient of the fittest member of the final population, and the denominator is the value $(\partial p/\partial t)_{\max} \approx 3.95\,\text{mPa/s}$ found in Section 3.1 in the absence of windows.

These results are typical of those obtained when the genetic algorithm is terminated after ~500 generations. The compression wave profiles in both cases exhibit smooth, linear pressure variations across the wave-front except for a small, localized inflexion at the foot of the wavefront, generated just as the nose enters the hood. Further calculation shows that this inflexion (and the corresponding fluctuation in the pressure gradient) is absent for ℓ_h/R smaller than about 4. The pressure gradients are uniformly small over the whole interval of the wave-front. In both cases the region

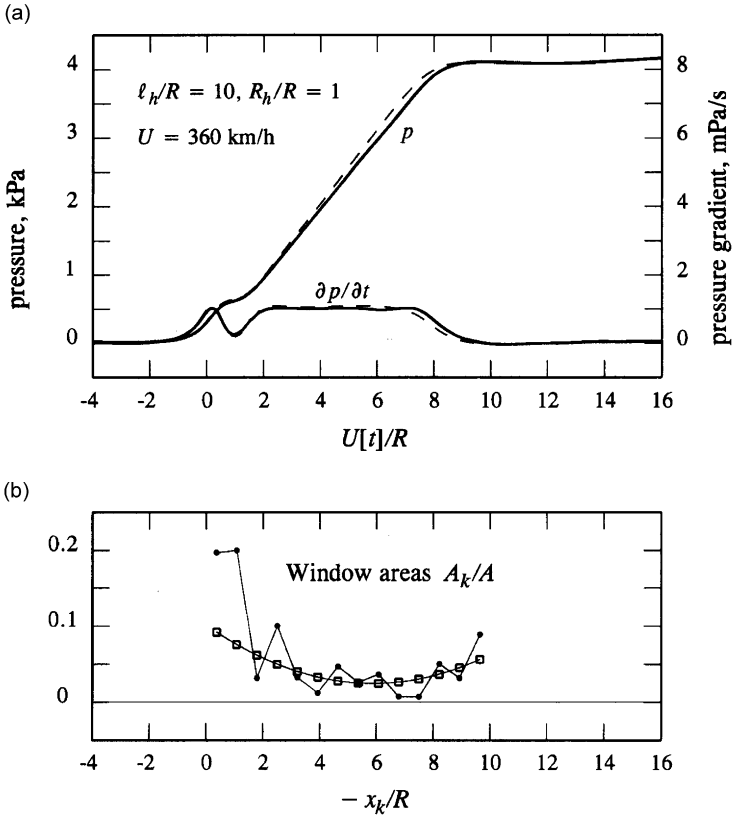

Fig. 6. (a) —: calculated optimal time dependances of the compression wave pressure p and pressure gradient $\partial p/\partial t$ for the model train defined by (2.1)–(2.3) for $U = 360\,\text{km/h}$, $\ell_h = 10R$, $R_h/R = 1$ and 14 'far' windows ($z_t = -0.4R$); the broken-line curves (– – –) are for the parabolic window distribution discussed in Section 4.2. (b) • • •: The corresponding window distribution (□ □ □, see Section 4.2).

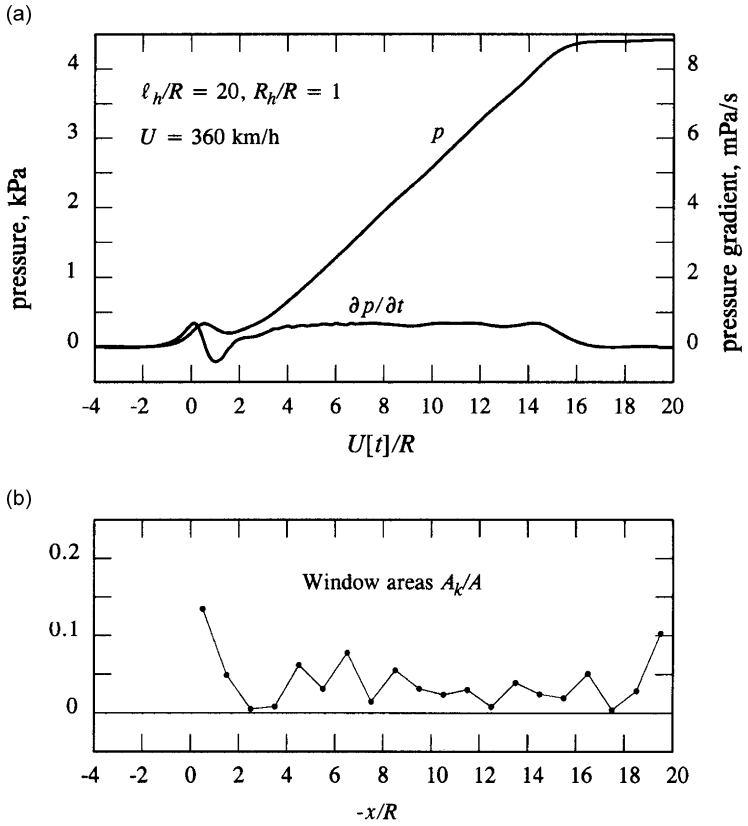

Fig. 7. (a) Calculated optimal time dependances of the compression wave pressure p and pressure gradient $\partial p/\partial t$ for the model train defined by (2.1)–(2.3) for $U = 360$ km/h, $\ell_h = 20R$, $R_h/R = 1$ and 20 'far' windows ($z_t = -0.4R$). (b) The corresponding window distribution.

Table 1
Minima of $(\partial p/\partial t)_{\max}$ predicted by the genetic algorithm

ℓ_h/R	N	z_t/R	$(\partial p/\partial t)_{\max}$ (mPa/s)	at $U[t]/R$	α
10	14	−0.4	1.030	0.21	0.26
20	20	−0.4	0.686	10.50	0.17

of uniform wave growth occurs over a 'retarded interval' of the hood of length $|\delta x|$ that is smaller than the nominal hood length ℓ_h occupied by the windows ($|\delta x|/R \sim 8, 16$, respectively, in Figs. 6 and 7). Also both figures indicate that relatively large windows are required at the inner end of the hood to provide a smooth transition from this rapid growth to the slow, drag dominated amplitude growth to the rear of the main wave-front.

The fluctuating nature of the window area distributions in Figs. 6(b) and 7(b) is consistent with our remark above concerning the large number of configurations with near optimal characteristics. It is interesting to note, however, that in both cases there are relatively large windows at the open end of the hood (i.e. at the portal). The efficiency with which a window near the portal affects the radiation into the tunnel is very small. Indeed, each window is acoustically equivalent to a monopole source that is necessarily accompanied by an equal and opposite 'image' source in the wall of the outside ('virtual') extension of the hood in order to satisfy the open end 'pressure release' condition (at $x = \ell_E$). A window very close to the entrance is therefore equivalent to a relatively weak 'compact' acoustic dipole, and must be large to make a finite contribution to the radiation in the tunnel.

The genetic algorithm must be applied several times for each value of ℓ_h/R and for a range of values of N. This permits a good approximation to be identified for the global minimum of $(\partial p/\partial t)_{\max}$, and the corresponding optimal values of the attenuation α can then be calculated from (4.2). The results of such a survey for the present case of 'far'

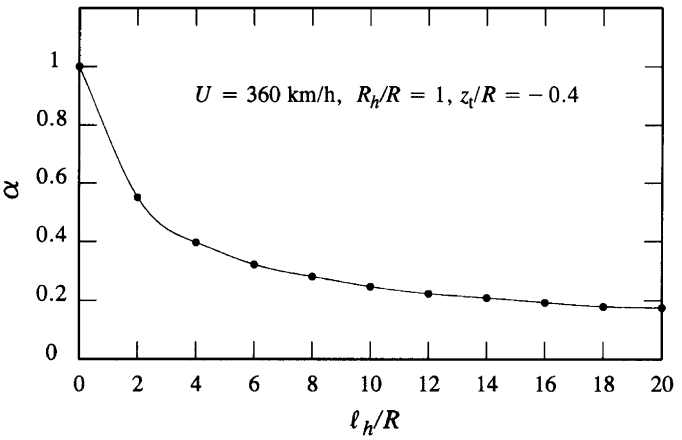

Fig. 8. Dependence on ℓ_h/R of the optimal value of the attenuation α for unconstrained far windows ($z_t = -0.4R$) when $U = 360\,\text{km/h}$, $R_h/R = 1$.

windows ($z_t = -0.4$) are presented in Fig. 8, which shows a sequence of calculated values of α (the solid circles •) interpolated by a smooth curve. The rapid decrease in α over the interval $0 < \ell_h < 2$ is reminiscent of the same behaviour in Fig. 5(b) for an unvented hood. The behaviour for longer hoods is very different, however, because the judiciously placed and sized windows continue to produce a slow but relentless reduction in α as the hood length ℓ_h increases, and compression wave profiles that are smooth and exhibit essentially linear growth across the wave-front.

4.2. Parabolically constrained windows

The smooth and continuous nature of the calculated data points in Fig. 8 gives some confidence in the convergence of the genetic algorithm to the global minimum of α. But the irregular variation of window sizes evident in Figs. 6 and 7 indicates that a very much larger number of numerical iterations is necessary to identify corresponding smoothly varying window distributions from among the irregular patterns that furnish very similar values of α. However, if the ultimate goal is the fabrication of an optimal hood, a more uniform distribution of window sizes is desirable, especially if it is required to construct a continuous window in the form of a long slit of slowly varying width.

Smoothly varying, *near-optimal* window distributions can be found by prescribing the window area distribution A_k as an appropriate function of x_k. Inspection of Figs. 6 and 7, for example, suggests that, when $R_h = R$, a convenient and simple distribution might be furnished by the parabola

$$\frac{A_k}{\mathscr{A}} = a\left(\frac{x_k}{R} + b\right)^2 + c, \quad a, c > 0. \tag{4.3}$$

This distribution is positive definite and takes its minimum value at $x_k/R = -b$. It can therefore be regarded (for $b > 0$) as providing a crude approximation to the irregular 'U-shaped' distributions of Figs. 6 and 7.

Optimization now reduces to the determination of the optimal values of the three coefficients a, b, c for any prescribed number of windows N and hood length ℓ_h/R. The genetic algorithm is modified in an obvious manner, by taking each window distribution to be defined by a string with three substrings, each respectively representing the values of a, b, c. Thus, the task for the genetic algorithm is very much reduced because, although optimization must still be performed over an infinity of possible window distributions, they form an infinite subset of dimension 3 of the entire ∞^N space of possible distributions. The results of such a calculation will be useful provided the subset includes members whose attenuation α closely approximates the corresponding optimum for unconstrained windows.

That this is indeed the case is seen by reference Fig. 9 and Table 2. The latter lists predicted values of α (and corresponding values of a, b, c) for parabolically constrained windows when $R_h/R = 1, z_t/R = -0.4$ and $U = 360\,\text{km/h}$. The figure shows that these values of α (• • •) are close to or coincide with the α-curve (—) for the unconstrained windows discussed in Section 4.1. Similarly, reference back to Fig. 6 indicates how predictions for constrained and unconstrained windows differ in detail. The broken line curves in Fig. 6(a) represent the pressure and pressure gradient profiles for 14 windows distributed parabolically when $\ell_h/R = 10$; the actual window distribution is shown in Fig. 6(b) (□ □ □). For practical purposes the predictions are identical. However, it should be noted that 14 windows distributed parabolically yield a minimum value of $(\partial p/\partial t)_{\max} \sim -1.09\,\text{mPa/s}$, for which $\alpha \approx 0.276$, marginally larger than the absolute

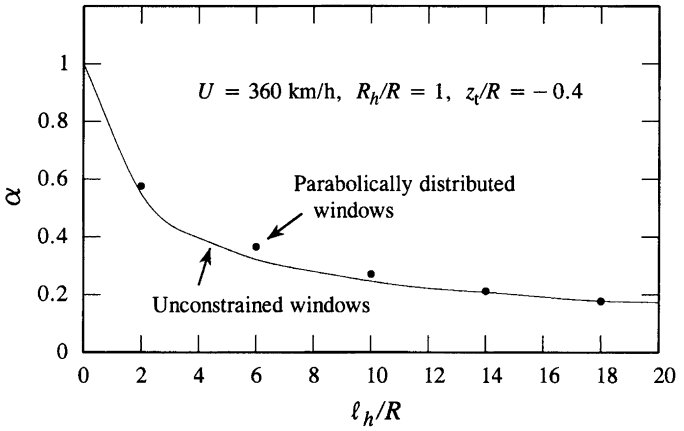

Fig. 9. Comparison of predicted optimal values of α for parabolically constrained windows (• • •, Table 2) and the predictions of Fig. 8 (—) for unconstrained windows for $z_t/R = -0.4$, $R_h/R = 1$, $U = 360$ km/h.

Table 2
Parabolically constrained far windows ($z_t/R = -0.4$, $R_h/R = 1$)

ℓ_h/R	N	α	a	b	c
2	10	0.576	0.09961	0.71373	0.01224
6	18	0.365	0.00941	3.48235	0.00519
10	20	0.271	0.00158	5.60784	0.01458
14	20	0.212	0.00088	8.01569	0.01693
18	18	0.177	0.00065	10.65882	0.02162

minimum given in Table 2 for $N = 20$ windows, but this is nonetheless very close to the 1.03 mPa/s obtained for unconstrained windows (Table 1).

5. Hood optimization for $R_h/R = 1.25$

5.1. Unconstrained near windows

Turn attention now to the optimization problem for the more general hood depicted in Fig. 2, for $R_h/R = 1.25$. The solid, 'unconstrained windows' curve in Fig. 10 shows the variation with ℓ_h/R of the optimized hood attenuation α for *near* windows ($z_t/R = 0.4$) when $U = 360$ km/h; also shown is the α-variation for $R_h/R = 1.25$ in the absence of windows (Section 3).

The calculated pressure and pressure gradient profiles are illustrated in Fig. 11(a) (—) for $\ell_h/R = 10$ when the hood is optimized using $N = 12$ near windows. As in the case $R_h/R = 1$ discussed in Section 3, there are many irregular window distributions that give near optimal behaviour for a prescribed value of N. However, they all exhibit the characteristic structure displayed for the present realisation in Fig. 11(b) (• • •), namely that the innermost windows are very small. In the present case, of the three innermost windows ($k = 10, 11, 12$) the window area A_{10} is small, and $A_{11} \sim A_{12} \approx 0$. Configurations of this kind, where windows adjacent to the hood-tunnel junction are effectively *shut*, are typical of all optimized distributions when ℓ_h/R exceeds about 3 or 4.

5.2. Chopped-parabolic near windows

These conclusions suggest that smoothly varying, near optimal window distributions might be obtained (for $R_h/R > 1$) by optimizing the following *chopped-parabolic* generalisation of the parabolic distribution (4.3):

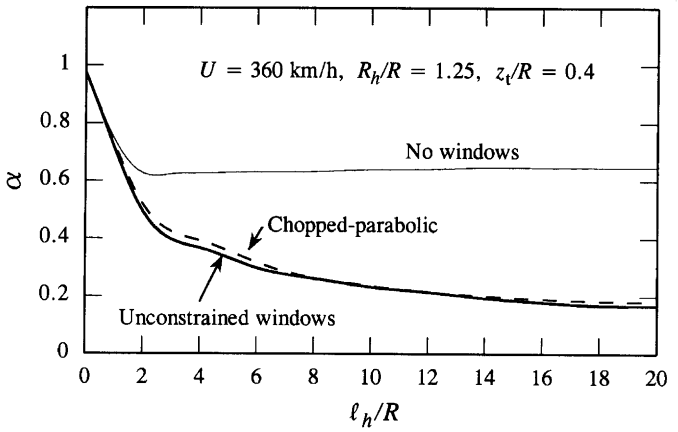

Fig. 10. Dependence on ℓ_h/R of the attenuation α for unconstrained (—) and chopped-parabolically constrained (– – –) near windows ($z_t = 0.4R$) when $U = 360\,\mathrm{km/h}$, $R_h/R = 1.25$.

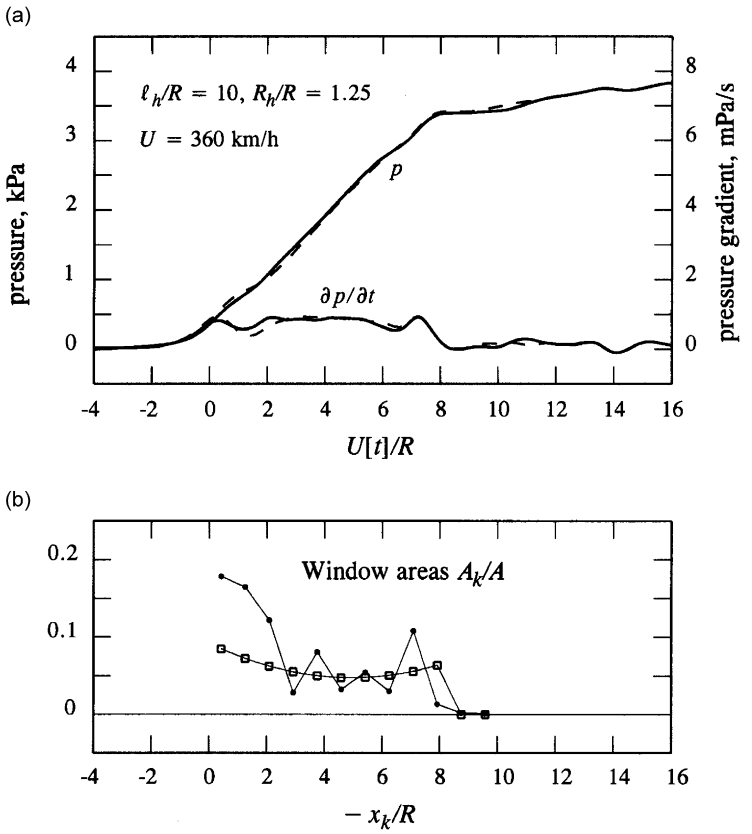

Fig. 11. (a) —-: calculated optimal time dependances of the compression wave pressure p and pressure gradient $\partial p/\partial t$ for the model train defined by (2.1)–(2.3) for $U = 360\,\mathrm{km/h}$, $\ell_h = 10R$, $R_h/R = 1.25$ and 12 near windows ($z_t = 0.4R$); the broken-line curves (– – –) are for the chopped-parabolic window distribution. (b) The corresponding unconstrained (• • •) and chopped-parabolically constrained (□ □ □) window distributions.

$$\frac{A_k}{\mathscr{A}} = \begin{cases} a(x_k/R + b)^2 + c, & 0 < -x_k/R < d, \\ 0, & d < -x_k/R < \ell_h/R, \end{cases} \qquad a, c, d > 0. \tag{5.1}$$

Table 3
Chopped-parabolically constrained near windows ($z_t/R = 0.4$, $R_h/R = 1.25$)

ℓ_h/R	N	α	a	b	c	d
2	4	0.518	0.09926	0.73637	0.00050	1.89827
4	4	0.392	0.02466	3.97656	0.02710	2.61490
6	6	0.316	0.00677	4.69890	0.06569	4.64147
8	10	0.264	0.00625	3.89744	0.05146	6.78720
10	10	0.236	0.00399	4.62271	0.05916	8.20855
12	12	0.214	0.00242	6.08445	0.05731	10.15385
14	12	0.201	0.00168	6.83419	0.06130	11.24992
16	14	0.191	0.00090	8.02149	0.06042	13.32747
18	16	0.184	0.00026	0.79560	0.03173	16.11341
20	18	0.183	0.00020	1.96078	0.03727	17.89804

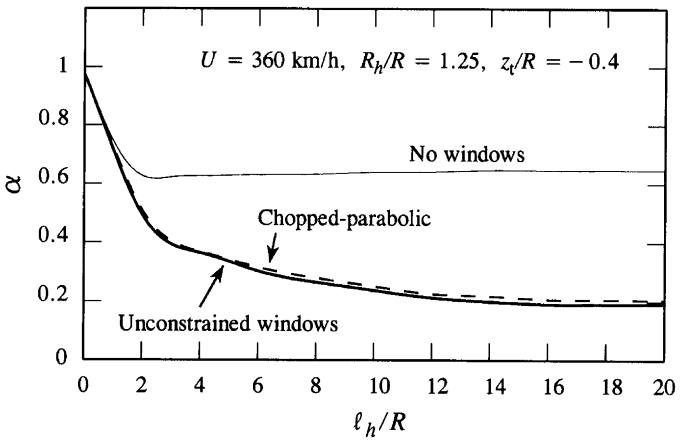

Fig. 12. Dependence on ℓ_h/R of the attenuation α for unconstrained (—) and chopped-parabolically constrained (– – –) far windows ($z_t = -0.4R$) when $U = 360\,\mathrm{km/h}$, $R_h/R = 1.25$.

Table 4
Chopped-parabolically constrained far windows ($z_t/R = -0.4$, $R_h/R = 1.25$)

ℓ_h/R	N	α	a	b	c	d
2	8	0.507	0.07339	0.43137	0.00050	1.77098
4	12	0.368	0.00633	3.24706	0.11942	2.42510
6	10	0.316	0.00537	−0.64029	0.09677	3.70432
8	16	0.280	0.00360	3.83101	0.03792	5.98701
10	14	0.252	0.00375	4.06105	0.05336	7.29035
12	18	0.227	0.00278	5.31765	0.04040	8.59294
14	10	0.219	0.00204	6.44444	0.11133	9.82222
16	8	0.208	0.00027	14.98413	0.16833	12.64762
18	8	0.207	0.00037	−5.01177	0.10142	13.96235
20	6	0.206	0.00100	−2.85714	0.09550	14.53968

Thus, all windows constrained in this way are shut when $-x_k/R > d$, and the genetic algorithm is required to minimize $(\partial p/\partial t)_{\max}$ with respect to the four parameters a, b, c, d.

Table 3 displays the optimal parameter values and the corresponding hood attenuation α for chopped-parabolic near windows ($z_t/R = 0.4$, $R_h/R = 1.25$, $U = 360\,\mathrm{km/h}$). The attenuation α, plotted as the broken line curve in Fig. 10, is seen to provide a close approximation to the predicted overall optimal behaviour for unconstrained windows. The pressure and pressure gradient profiles for $\ell_h/R = 10, N = 12$ are also plotted as broken line curves in Fig. 11(a); these plots are negligibly different from the corresponding prediction for unconstrained near windows. Fig. 11(b) compares

the corresponding smoothly varying, chopped-parabolic window distribution (□ □ □) with that (• • •) for 12 unconstrained windows. The chopped-parabolic windows $k = 11, 12$ are *shut*.

5.3. Far windows

Similar predictions for the optimal attenuation α are obtained when $R_h/R = 1.25$ for 'far' windows ($z_t/R = -0.4$). The solid-line curve (—) in Fig. 12 illustrates this for unconstrained windows. Once again it is found that optimal window areas A_k close to the junction of the hood and tunnel are very small or negligible, so that smoothly varying, near optimal window distributions can be realised by optimizing the chopped-parabola formula (5.1). The results of such an investigation are given in Table 4 and plotted as the broken-line curve in Fig. 12.

6. Conclusion

The subjective impact of the compression wave generated when a train enters a tunnel is governed by the magnitude of the peak pressure gradient $(\partial p/\partial t)_{\max}$. Tunnel entrance hoods are used to elongate the front of the compression wave and thereby diminish the value of $(\partial p/\partial t)_{\max}$. The simplest type of hood consists of a uniform tunnel extension whose cross-section $\mathscr{A}_h$ exceeds the tunnel cross-section $\mathscr{A}$; wave trapping by multiple reflections from the ends of the hood then cause the compression wave-front to rise in stages with reduced maximum pressure gradient equal to a fraction α (<1) of the pressure gradient in the absence of the hood. The value of α decreases rapidly as the hood length ℓ_h increases from zero, but for a given value of the area ratio $\mathscr{A}_h/\mathscr{A}$ it attains a minimum and remains approximately constant with further increases in ℓ_h. Thus, in the case of the circular cylindrical model scale hoods and tunnels studied in this paper the minimum value $\alpha \approx 0.6$ is reached at $\ell_h \sim 2R$ when $\mathscr{A}_h/\mathscr{A} = 1.5625$ ($R_h/R = 1.25$).

The simplest and most effective way to achieve further reductions in α is to line one or both of the hood walls with a sequence of 'open windows'. Current practice for train speeds up to about 300 km/h is to use relatively short hoods with windows, namely hoods that correspond at model scale to ℓ_h less than about $4R$. In such cases it is feasible to determine the window distribution and sizing by experiment. At higher speeds, however, longer hoods are needed and design by experiment becomes a much lengthier and more tedious process. The numerical optimization scheme of this paper should then prove useful. The method yields near-optimal, smoothly varying parabolic or chopped-parabolic window distributions for long hoods (ℓ_h as large as $20R$), respectively, for $\mathscr{A}_h/\mathscr{A} = 1$ and $\mathscr{A}_h/\mathscr{A} > 1$, and for which the optimum value of α is reduced to about 0.2–0.25. The procedure can be used to design hoods with discrete windows or, by performing the numerical optimization using a large number of relatively small windows, it can determine the optimal variation of the width of a window in the form of a long slit cut in the side of the hood.

To appreciate further the power of the method it might be noted that running the genetic algorithm through 500 generations with a population size $N_{\text{pop}} = 16$ involves 8000 separate fitness calculations, equivalent to 8000 experimental test runs. Moreover, if there are 10 unconstrained windows and the area of each is represented by an 8 bit binary string, the optimized window distribution is extracted by the genetic algorithm from amongst a total of $\sim 1.2 \times 10^{24}$ different possibilities.

Our results also indicate that the overall optimal compression waveform in a long hood is attained when $\mathscr{A}_h = \mathscr{A}$, when there are no reflections from the change in cross-sectional area at the junction of the hood and tunnel. The compression wave exhibits growth that is essentially smooth and linear across the whole of the wavefront except for a small localized inflexion generated just as the train nose enters the hood. For this case the maximum pressure gradient is also smaller than for $\mathscr{A}_h/\mathscr{A} = 1.5625$ provided ℓ_h/R exceeds about 12.

Acknowledgement

The work reported in this paper is sponsored by the Railway Technical Research Institute, Tokyo, Japan.

Appendix A. Formulae for the compression wave

The various components of the pressure in (2.4) depend in the first instance on geometrical properties of the hood and the junction which, when the presence of the windows is temporarily ignored, are determined by two particular solutions $\varphi^*_{\text{E}}(\mathbf{x}), \varphi^*_{\text{J}}(\mathbf{x})$ of Laplace's equation. The function $\varphi^*_{\text{E}}(\mathbf{x})$ represents the velocity potential of a hypothetical,

uniform incompressible flow *out* of the hood portal normalized such that

$$\left.\begin{aligned}\varphi_{\rm E}^*(\mathbf{x}) &\approx x-\ell_{\rm E} \quad \text{for } |x|\gg R_h \quad \text{inside the hood,}\\ &\approx -\mathscr{A}_h/4\pi|\mathbf{x}| \quad \text{for } |\mathbf{x}|\gg R_h \quad \text{in free space outside the hood,}\end{aligned}\right\} \tag{A.1}$$

where $\ell_{\rm E}\approx 0.61R_h$ is the Rayleigh *end-correction* (Rayleigh, 1926; Howe, 1998).

The harmonic function $\varphi_{\rm J}^*(\mathbf{x})$ represents a steady potential flow through the junction from the tunnel to the hood. When the hood length $\ell_h>2R_h$ its behaviour in the neighbourhood of J is well approximated by the solution of Laplace's equation obtained by assuming the hood to extend to $x=+\infty$, and is normalized such that

$$\left.\begin{aligned}\varphi_{\rm J}^*(\mathbf{x}) &\approx x+\ell_h-\ell_{\rm J} \quad \text{for } x+\ell_h\to-\infty \text{ in the tunnel,}\\ &\approx \frac{\mathscr{A}}{\mathscr{A}_h}(x+\ell_h) \quad \text{for } x+\ell_h\to+\infty \text{ in the hood.}\end{aligned}\right\} \tag{A.2}$$

The length $\ell_{\rm J}$ is the effective 'hydrodynamic length' of the junction; it is usually negligible (Howe et al., 2003a).

The following reflection and transmission coefficients $\mathscr{R}_{\rm J}$, $\mathscr{T}_{\rm J}$, respectively, determine the amplitude of a wave reflected *back into* the hood at the junction J, and transmitted across the junction into the tunnel (into $x<-\ell_h$):

$$\mathscr{R}_{\rm J}=\frac{\mathscr{A}_h-\mathscr{A}}{\mathscr{A}_h+\mathscr{A}}, \quad \mathscr{T}_{\rm J}=\frac{2\mathscr{A}_h}{\mathscr{A}_h+\mathscr{A}}. \tag{A.3}$$

Primitive hood-entrance and junction-generated waves $P_{\rm E}, P_{\rm JT}, P_{\rm JH}$ are defined as follows:

$$P_{\rm E}\left(t+\frac{x}{c_0}\right)\approx\frac{\rho_0U^2}{\mathscr{A}_h(1-M^2)}\left(1+\frac{\mathscr{A}_0}{\mathscr{A}}\right)\int_{-\infty}^{\infty}\frac{\partial\varphi_{\rm E}^*}{\partial x'}(x',0,z_{\rm t})\frac{\partial\mathscr{A}_{\rm T}}{\partial x'}\left(x'+U\left(t+\frac{x-\ell_{\rm E}}{c_0}\right)\right)\mathrm{d}x', \tag{A.4}$$

where $M=U/c_0$ is the train Mach number,

$$\begin{aligned}P_{\rm JT}\left(t+\frac{x}{c_0}\right)=&\frac{\rho_0U^2}{(1-M^2)}\frac{\mathscr{A}_0}{\mathscr{A}}\left(1+\frac{\mathscr{A}_0}{\mathscr{A}}\right)\frac{\mathscr{T}_{\rm J}}{2}\\ &\times\left\{\int_{-\infty}^{\infty}\frac{\partial\varphi_{\rm J}^*}{\partial x'}(x',0,z_{\rm t})\frac{\partial\mathscr{A}_{\rm T}}{\partial x'}\left(x'+U\left(t+\frac{x+\ell_h}{c_0}\right)\right)\frac{\mathrm{d}x'}{\mathscr{A}_0}-\frac{\mathscr{A}}{\mathscr{A}_h}\right\}, \quad x<-\ell_h;\end{aligned} \tag{A.5}$$

and

$$\begin{aligned}P_{\rm JH}\left(t-\frac{x}{c_0}\right)=&\frac{-\rho_0U^2}{(1-M^2)}\frac{\mathscr{A}_0}{\mathscr{A}_h}\left(1+\frac{\mathscr{A}_0}{\mathscr{A}}\right)\frac{\mathscr{T}_{\rm J}}{2}\\ &\times\left\{\int_{-\infty}^{\infty}\frac{\partial\varphi_{\rm J}^*}{\partial x'}(x',0,z_{\rm t})\frac{\partial\mathscr{A}_{\rm T}}{\partial x'}\left(x'+U\left(t-\frac{x+\ell_h}{c_0}\right)\right)\frac{\mathrm{d}x'}{\mathscr{A}_0}-\frac{\mathscr{A}}{\mathscr{A}_h}\right\}, \quad -\ell_h<x<0.\end{aligned} \tag{A.6}$$

The pressure components $p_{\rm E}(x,t), p_{\rm J}(x,t)$ on the right of (2.4) are then given by

$$p_{\rm E}(x,t)=\mathscr{T}_{\rm J}\sum_{n=0}^{\infty}(-\mathscr{R}_{\rm J})^nP_{\rm E}\left(t+\frac{x}{c_0}-\frac{2n(\ell_h+\ell_{\rm E})}{c_0}\right), \quad x<-\ell_h; \tag{A.7}$$

$$p_{\rm J}(x,t)=P_{\rm JT}\left(t+\frac{x}{c_0}\right)-\mathscr{T}_{\rm J}\sum_{n=0}^{\infty}(-\mathscr{R}_{\rm J})^nP_{\rm JH}\left(t+\frac{x}{c_0}-\frac{2n(\ell_h+\ell_{\rm E})}{c_0}-\frac{2\ell_{\rm E}}{c_0}\right), \quad x<-\ell_h. \tag{A.8}$$

These formulae are applicable provided the hood length ℓ_h is large enough for the potential flows represented by $\varphi_{\rm E}^*$ and $\varphi_{\rm J}^*$ to be good approximations to the potential of an incompressible flow from the tunnel and out of the hood. This condition obviously fails for a 'flanged exit' (when $\ell_h=0$), and is probably invalid also for ℓ_h smaller than about R_h. In these cases we take

$$p_{\rm E}(x,t)=P_{\rm E}\left(t+\frac{x}{c_0}\right), \quad p_{\rm J}(x,t)=0, \tag{A.9}$$

where $P_{\rm E}$ is defined as in (A.4) with the conditions (A.1) replaced by

$$\left.\begin{aligned}\varphi_{\rm E}^*(\mathbf{x}) &\approx x-\ell_{\rm E} \quad \text{for } |x|\gg R \quad \text{inside the tunnel,}\\ &\approx -\mathscr{A}/4\pi|\mathbf{x}| \quad \text{for } |\mathbf{x}|\gg R_h \quad \text{in free space outside the hood;}\end{aligned}\right\} \tag{A.10}$$

the end correction $\ell_{\rm E}$ must now be determined numerically along with $\varphi_{\rm E}^*(\mathbf{x})$.

The drag-generated pressure $p_{\rm D}(x,t)$ in (2.4) is given by

$$p_{\rm D}(x,t) = p_{\rm DH}(x,t) + p_{\rm DT}(x,t), \tag{A.11}$$

where

$$\begin{aligned} p_{\rm DH}(x,t) = \frac{\mu^2\rho_0}{2\mathscr{A}_h}(L_{R_h}U_{\rm HW}^2 + L_hU_{\rm HT}^2)\Bigg\{&\Bigg[\left(\frac{U(t+x/c_0)-L-M(\ell_{\rm D}-\ell_{\rm E}\mathscr{A}/\mathscr{A}_h)}{1-M\mathscr{A}/\mathscr{A}_h}\right)_+ \\ &-\left(\frac{U(t+x/c_0)-L-M(\ell_{\rm D}-\ell_{\rm E}\mathscr{A}/\mathscr{A}_h)}{1-M\mathscr{A}/\mathscr{A}_h}-\ell_h\right)_+\Bigg] \\ &+\Bigg[\left(\frac{U(t+x/c_0)-L-M(\ell_{\rm D}+\ell_{\rm E}\mathscr{A}/\mathscr{A}_h)}{1+M\mathscr{A}/\mathscr{A}_h}\right)_+ \\ &-\left(\frac{U(t+x/c_0)-L-M(\ell_{\rm D}+\ell_{\rm E}\mathscr{A}/\mathscr{A}_h)}{1+M\mathscr{A}/\mathscr{A}_h}-\ell_h\right)_+\Bigg]\Bigg\}, \end{aligned} \tag{A.12}$$

$$p_{\rm DT}(x,t) = \frac{\mu^2\rho_0}{2\mathscr{A}}(L_RU_{\rm TW}^2 + L_hU_{\rm TT}^2)\left\{\left(\frac{U(t+x/c_0)-L}{1-M}-\ell_h\right)_+ + \left(\frac{U(t+x/c_0)-L-2M\ell_{\rm D}}{1+M}-\ell_h\right)_+\right\}, \tag{A.13}$$

where μ is a constant 'friction factor', the function $(x)_+ = x, 0$ according as $x \gtrless 0$,

$$L_{R_h} = 2\pi R_h, \quad L_R = 2\pi R, \quad L_h = 2\pi h, \tag{A.14}$$

are respectively, the perimeters of the hood, tunnel and uniform section of the train, and

$$\begin{aligned} U_{\rm TW} &= \frac{\mathscr{A}_0U}{(\mathscr{A}-\mathscr{A}_0)}\left\{1-\frac{M\mathscr{A}}{(\mathscr{A}-\mathscr{A}_0)}+\frac{M^2\mathscr{A}(2\mathscr{A}-\mathscr{A}_0)}{2(\mathscr{A}-\mathscr{A}_0)^2}\right\}, \\ U_{\rm HW} &= \frac{\mathscr{A}_0U}{(\mathscr{A}_h-\mathscr{A}_0)}\left\{1-\frac{M\mathscr{A}_h}{(\mathscr{A}_h-\mathscr{A}_0)}+\frac{M^2\mathscr{A}_h(2\mathscr{A}_h-\mathscr{A}_0)}{2(\mathscr{A}_h-\mathscr{A}_0)^2}\right\}, \\ U_{\rm TT} &= \frac{\mathscr{A}U}{(\mathscr{A}-\mathscr{A}_0)}\left\{1-\frac{M\mathscr{A}_0}{(\mathscr{A}-\mathscr{A}_0)}+\frac{M^2\mathscr{A}_0(2\mathscr{A}-\mathscr{A}_0)}{2(\mathscr{A}-\mathscr{A}_0)^2}\right\}, \\ U_{\rm HT} &= \frac{\mathscr{A}_hU}{(\mathscr{A}_h-\mathscr{A}_0)}\left\{1-\frac{M\mathscr{A}_0}{(\mathscr{A}_h-\mathscr{A}_0)}+\frac{M^2\mathscr{A}_0(2\mathscr{A}_h-\mathscr{A}_0)}{2(\mathscr{A}_h-\mathscr{A}_0)^2}\right\}. \end{aligned} \tag{A.15}$$

Experiment (Howe and Iida, 2003; Howe et al., 2006) indicates that excellent predictions of $p_{\rm D}$ are obtained in model scale applications with U as large as 425 km/h by taking $\mu\sim0.053$. But there is no Reynolds number similarity between full scale and model scale, so that model scale predictions of $p_{\rm D}$ will not necessarily constitute satisfactory predictions for the drag-generated pressure at full scale.

The component $p_{\rm W}(x,t)$ of the compression wave attributable to the N windows can be cast in the form

$$p_{\rm W}(x,t) = \sum_{k=1}^{N} p_k(x,t), \quad x < -\ell_h, \tag{A.16}$$

where the pressure $p_k(x,t)$ generated by the kth window is given in terms of the mean exit flow velocity $V_k(t)$ (directed out of the kth window) by

$$\begin{aligned} p_k(x,t) = -\frac{\rho_0c_0A_k}{2\mathscr{A}_h}\mathscr{T}_{\rm J}\sum_{n=0}^{\infty}(-\mathscr{R}_{\rm J})^n\Bigg\{&V_k\left(t+\frac{\{x-x_k-2n(\ell_h+\ell_{\rm E})\}}{c_0}\right) \\ &-V_k\left(t+\frac{\{x+x_k-2n(\ell_h+\ell_{\rm E})-2\ell_{\rm E}\}}{c_0}\right)\Bigg\}. \end{aligned} \tag{A.17}$$

The N velocities $V_k(t)$ are determined by the following system of equations (Cummings, 1984, 1986)

$$\left.\begin{aligned} &\bar{\ell}_k(t)\rho_0\frac{{\rm d}V_k}{{\rm d}t}+\frac{\rho_0V_k|V_k|}{2\sigma^2} = p_{\rm I}(x_k,t)+\sum_{j=1}^{N}p_j(x_k,t) \\ &\frac{{\rm d}\mathscr{L}_k}{{\rm d}t} = |V_k(t)| \\ &\bar{\ell}_k(t) = \frac{\pi R_k}{4}+\left(\ell_w+\frac{\pi R_k}{4}\right)\Big/\left[1+\frac{1}{3}\left(\frac{\mathscr{L}_k}{2R_k}\right)^{1.585}\right] \end{aligned}\right\}, \quad k=1,2,\ldots,N. \tag{A.18}$$

New quantities on the right of these equations are defined as follows:

$$p_{\rm I}(x_k,t)=\hat{p}_{\rm E}(x_k,t)+\hat{p}_{\rm I}(x_k,t)+\hat{p}_{\rm J}(x_k,t), \tag{A.19}$$

where

$$\hat{p}_{\rm E}(x,t)=\sum_{n=1}^{\infty}(-\mathscr{R}_{\rm J})^n P_{\rm E}\left(t+\frac{x}{c_0}-\frac{2n(\ell_h+\ell_{\rm E})}{c_0}\right)+\mathscr{R}_{\rm J}\sum_{n=0}^{\infty}(-\mathscr{R}_{\rm J})^n P_{\rm E}\left(t-\frac{x}{c_0}-\frac{2n(\ell_h+\ell_{\rm E})}{c_0}-\frac{2\ell_h}{c_0}\right); \tag{A.20}$$

$$\begin{aligned}\hat{p}_{\rm I}(x_k,t)=&P_{\rm E}\left(t+\frac{x_k}{c_0}\right)\left\{1-\int_{-\infty}^{\infty}\frac{\mathscr{A}_{\rm T}(x')}{\mathscr{A}_0}\Psi(Ut+x_k-x',z_{\rm t})\,{\rm d}x'\right\}\\&+\begin{cases}p_{\rm DH}(x_k,t), & t<\dfrac{(-x_k+L)}{U},\\ p_{\rm DH}\left(x_k,\dfrac{(-x_k+L)}{U}\right), & t>\dfrac{(-x_k+L)}{U},\end{cases}\end{aligned} \tag{A.21}$$

in which

$$\Psi(x,z_{\rm t})=\frac{1}{\pi R_h\sqrt{1-M^2}}\sum_{n=0}^{\infty}\int_0^{\infty}\frac{\hat{\sigma}_n\lambda {\rm I}_n(\lambda|z_{\rm t}|/R_h)}{{\rm I}_{n-1}(\lambda)+{\rm I}_{n+1}(\lambda)}\cos\left(\frac{\lambda x}{R_h\sqrt{1-M^2}}\right){\rm d}\lambda \tag{A.22}$$

and

$$\hat{\sigma}_n=\begin{cases}1, & n=0,\\ 2, & n\geqslant 1 \text{ and } z_{\rm t}>0,\\ 2(-1)^n, & n\geqslant 1 \text{ and } z_{\rm t}<0;\end{cases} \tag{A.23}$$

$$\hat{p}_{\rm J}(x,t)=\sum_{n=0}^{\infty}(-\mathscr{R}_{\rm J})^n\left\{P_{\rm JH}\left(t-\frac{x}{c_0}-\frac{2n(\ell_h+\ell_{\rm E})}{c_0}\right)-P_{\rm JH}\left(t+\frac{x}{c_0}-\frac{2n(\ell_h+\ell_{\rm E})}{c_0}-\frac{2\ell_{\rm E}}{c_0}\right)\right\}; \tag{A.24}$$

and (for $-\ell_h<x<0$)

$$\begin{aligned}p_j(x,t)=&-\frac{\rho_0 c_0 A_j}{2\mathscr{A}_h}V_j\left(t-\frac{|x-x_j|}{c_0}\right)-\frac{\rho_0 c_0 A_j}{2\mathscr{A}_h}\sum_{n=0}^{\infty}(-\mathscr{R}_{\rm J})^n\left\{-V_j\left(t+\frac{\{x+x_j-2n(\ell_h+\ell_{\rm E})-2\ell_{\rm E}\}}{c_0}\right)\right.\\&+\chi_n V_j\left(t+\frac{\{x-x_j-2n(\ell_h+\ell_{\rm E})\}}{c_0}\right)+\chi_n V_j\left(t+\frac{\{-x+x_j-2n(\ell_h+\ell_{\rm E})\}}{c_0}\right)\\&\left.+\mathscr{R}_{\rm J}V_j\left(t-\frac{\{x+x_j+2n(\ell_h+\ell_{\rm E})+2\ell_h\}}{c_0}\right)\right\},\end{aligned} \tag{A.25}$$

where

$$\chi_n=\begin{cases}0, & n=0,\\ 1, & n\geqslant 1.\end{cases} \tag{A.26}$$

The constant σ in (A.18) is the effective contraction ratio of the window jets, which to a good approximation can be assumed to be constant and equal to 0.75 (Cummings, 1984, 1986); $\mathscr{L}_k$ is the axial length of the jet exhausting from the kth window, and $R_k=\sqrt{A_k/\pi}$ is the equivalent radius of the kth window (Cummings, 1984, 1986; Howe, 2005). The *causal* solution of these equations is required, subject to $V_k(t)=0, \mathscr{L}_k(t)=0$ $(k=1,2,\ldots,N)$ for t large and negative; the jet length $\mathscr{L}_k(t)$ must be reset to zero at every zero crossing of $V_k(t)$ (when the flow through the window reverses direction).

References

Auvity, B., Bellenoue, M. 1998 Vortex structure generated by a train-tunnel entry near the portal. Paper presented at the 8th International Symposium on Flow Visualization, Sorrento, Italy, 1–4 September 1998.

Auvity, B., Bellenoue, M., Kageyama, T., 2001. Experimental study of the unsteady aerodynamic field outside a tunnel during train entry. Experiments in Fluids 30, 221–228.

Carroll, D.L., 1996. Genetic algorithms and optimizing chemical oxygen–iodine lasers. Developments in Theoretical and Applied Mechanics 18, 411–424 (Wilson, H., Batra, R., Bert, C., Davis, A., Schapery, R., Stewart, D., Swinson, F. (Eds.) School of Engineering, University of Alabama, USA).

Coley, D.A., 1999. Genetic Algorithms for Scientists and Engineers. World Scientific Publishing Co., Singapore.

Cummings, A., 1984. Acoustic nonlinearities and power losses at orifices. American Institute of Aeronautics and Astronautics Journal 22, 786–792.

Cummings, A., 1986. Transient and multiple frequency sound transmission through perforated plates at high amplitude. Journal of the Acoustical Society of America 79, 942–951.

Fisher, R.A., 1958. The Genetical Theory of Natural Selection. Dover Publications, New York.

Fukuda, T., Iida, M., Suzuki, M., 2003. Visualization of unsteady flow generated by a train entering a tunnel. In: Proceedings of Utsunomiya Visualization Symposium, the Visualization Society of Japan, Utsunomiya, Japan, 31 October–1 November 2003, pp. 63–66.

Gawthorpe, R.G., 1978. Aerodynamics of trains in tunnels. Railway Engineer International 3, 41–47.

Goldberg, D.E., 1988. Genetic Algorithm in Search, Optimization and Machine Learning. Addison-Wesley, Reading, MA.

Gregoire, R., Rety, J.M., Moriniere, V., Bellenoue, M., Kageyama, T., 1997. Experimental study (scale $\frac{1}{70}$th) and numerical simulations of the generation of pressure waves and micro-pressure waves due to high-speed train-tunnel entry, pp. 877–902 of In: Gillard, J.R. (Ed.), Proceedings of the 9th International Conference on Aerodynamics and Ventilation of Vehicle Tunnels, Aosta Valley, Italy, 6–8 October 1997. ME Publications, London.

Howe, M.S., 1998. Acoustics of Fluid-Structure Interactions. Cambridge University Press, Cambridge.

Howe, M.S., 2005. On the role of separation in compression wave generation by a train entering a tunnel hood with a window. Institute of Mathematics and its Applications, Journal of Applied Mathematics 70, 400–418.

Howe, M.S., Iida, M., 2003. Influence of separation on the compression wave generated by a train entering a tunnel. International Journal of Aeroacoustics 2, 13–33.

Howe, M.S., Iida, M., Fukuda, T., Maeda, T., 2000. Theoretical and experimental investigation of the compression wave generated by a train entering a tunnel with a flared portal. Journal of Fluid Mechanics 425, 111–132.

Howe, M.S., Iida, M., Fukuda, T., 2003a. Influence of an unvented tunnel entrance hood on the compression wave generated by a high-speed train. Journal of Fluids and Structures 17, 833–853.

Howe, M.S., Iida, M., Fukuda, T., Maeda, T., 2003b. Aeroacoustics of a tunnel-entrance hood with a rectangular window. Journal of Fluid Mechanics 487, 211–243.

Howe, M.S., Iida, M., Maeda, T., Sakuma, Y., 2006. Rapid calculation of the compression wave generated by a train entering a tunnel with a vented hood. Journal of Sound and Vibration 297, 267–292.

Iida, M., 2005. Private communication regarding experiments performed at the Railway Technical Institute, Tokyo.

Iida, M., Matsumura, T., Nakatani, K., Fukuda, T., Maeda, T., 1996. Optimum nose shape for reducing tunnel sonic boom. Institution of Mechanical Engineers Paper C514/015/96.

Ito, M., 2000. Improvement to the aerodynamic characteristics of Shinkansen rolling stock. Proceedings of the Institution of Mechanical Engineers Part F, Journal of Rail and Rapid Transit 214, 135–143.

Maeda, T., Matsumura, T., Iida, M., Nakatani, K., Uchida, K., 1993. Effect of shape of train nose on compression wave generated by train entering tunnel. In: Iguchi, M. (Ed.), Proceedings of the International Conference on Speedup Technology for Railway and Maglev Vehicles, Yokohama, Japan, 22–26 November 1993, pp. 315–319.

Matsuo, K., Aoki, T., Mashimo, S., Nakatsu, E., 1997. Entry compression wave generated by a high-speed train entering a tunnel. In: Gillard, J.R. (Ed.), Proceedings of the 9th International Conference on Aerodynamics and Ventilation of Vehicle Tunnels, Aosta Valley, Italy, 6–8 October 1997. ME Publications, London, pp. 925–934.

Michalawicz, Z., 1992. Genetic Algorithms+Data Structures = Evolution Programs. Springer, Berlin.

Noguchi, Y., Okamura, Y., Uchida, K., Ishihara, T., Mashimo, S., Kageyama, M., 1996. Solving aerodynamic environmental problems arising from train speed-up. Institution of Mechanical Engineers Paper C514/039/96.

Ozawa, S., Maeda, T., 1988a. Tunnel entrance hoods for reduction of micro-pressure wave. Quarterly Report of the Railway Technical Research Institute 29, 134–139.

Ozawa, S., Maeda, T., 1988b. Model experiment on reduction of micro-pressure wave radiated from tunnel exit. In: Emori, R.I. (Ed.), Proceedings of the International Symposium on Scale Modeling, Tokyo, 18–22 July 1988. Seikei University, Japan Society of Mechanical Engineers, pp. 33–37.

Ozawa, S., Morito, Y., Maeda, T., Kinosita, M., 1976. Investigation of the pressure wave radiated from a tunnel exit. Railway Technical Research Institute Report No. 1023, 1976 (in Japanese).

Ozawa, S., Uchida, T., Maeda, T., 1978. Reduction of micro-pressure wave radiated from tunnel exit by hood at tunnel entrance. Quarterly Report of the Railway Technical Research Institute 19 (2), 77–83.

Ozawa, S., Maeda, T., Matsumura, T., Uchida, K., Kajiyama, H., Tanemoto, K., 1991. Countermeasures to reduce micro-pressure waves radiating from exits of Shinkansen tunnels. In: Haerter, A. (Ed.), Aerodynamics and Ventilation of Vehicle Tunnels. Elsevier Science, Amsterdam, pp. 253–266.

Peters, J.L., 2000. Tunnel optimized train nose shape. Paper presented at the 10th International Symposium on Aerodynamics and Ventilation of Vehicle Tunnels, Boston, USA, 1–3 November 2000.

Rayleigh, L., 1926. The Theory of Sound, vol. 2. Macmillan, London.

Vose, M.D., 1999. The Simple Genetic Algorithm. MIT Press, Cambridge, MA.

Winslow, A., Howe, M.S., Iida, M., 2005. Influence of a scarfed portal on the compression wave generated by a high-speed train entering a tunnel. Journal of Low Frequency Noise, Vibration and Active Control 24, 203–217.

Woods, W.A., Pope, C.W., 1976. Secondary aerodynamic effects in rail tunnels during vehicle entry. In: Second BHRA Symposium of the Aerodynamics and Ventilation of Vehicle Tunnels, Cambridge, England, 23–25 March 1976, Paper C5, pp. 71–86.